Efficient True Resistivity Prediction and Time Optimization in PcRI Measurements: A Results-Driven Approach

Meysam Nourani*, *Alvaro* Munoz Beltran, *Stefano* Pruno and *Hans-Erik* Rodvelt

Stratum Reservoir AS, Stavanger, Norway

Abstract. This study aims to validate models developed for predicting true resistivity and water saturation in drainage capillary pressure and formation resistivity index (PcRI) measurements using porous plate methodology. The true resistivity model enables the calculation of the time required to reach equilibrium for these key parameters. To validate the petrophysical resistivity model, an extensive database was used, comprising over 12,500 data points collected from sandstone and carbonate rocks analysed under various fluid systems, including crude oil/water, laboratory oil/water, and gas/water. The true resistivity and water production models reliably estimated true resistivity and water saturation as a function of time for both rock types. Based on transient drainage PcRI data, the models can predict equilibrium true resistivity and water production, significantly reducing measurement time and accelerating PcRI measurements by up to 63% in some cases. This optimization improves analysis timing and facilitates data interpretation, making the models as an important tool for enhancing efficiency in laboratory PcRI analysis. These models also have practical applications in monitoring and controlling the quality of transient drainage PcRI data. Additionally, they support the interpretation and validation of results, ensuring a more reliable and robust petrophysical evaluation.

Introduction

Capillary pressure and resistivity index (PcRI) are important variables in reservoir characterization obtained through porous plate experiments [1–3]. Using these parameters in reservoir simulation models will aid in predicting fluid flow and distribution in the reservoir [1,4]. It is widely recognized that the porous plate technique, also known as the equilibrium method, can be used simultaneously to determine both the capillary pressure and water saturation-resistivity index (S_w-RI) relationship according to the saturation history. In contrast to other methods, the porous plate method directly measures these relationships without requiring model-based calculations. As a direct measurement, this is an advantage. However, the main disadvantage is the time investment required due to the low flux through the porous plate [1]. As a result, this limitation is particularly evident in rocks with low ($1\ mD < K < 10\ mD$) or very low permeability ($K < 1\ mD$), where achieving equilibrium can take a considerable amount of time, even months or more to complete [3,5,6].

Due to the limitation of the traditional porous plate method, alternative methods may be considered. There are several alternative methods available, including Membrane Technique (MT), Continuous Injection (CI), Mercury Injection Capillary Pressure (MICP), Centrifuge, Digital Rock Physics (DRP), Pore Network Modelling (PNM), Artificial Neural Networks (ANNs), and even using Fractal Theory (FT) in capillary pressure prediction [5,7–13].

In MT experiments, thin microporous membranes help reduce experimental duration by minimizing the influence of membrane permeability. However, these membranes struggle to withstand mechanical stress and to maintain their wettability throughout the experiment [1,14].

CI determines the resistivity index as a function of water saturation. While it shares similarities with the porous plate technique, it differs in that it utilizes an ultra low constant injection rate rather than applying a stepwise constant differential pressure. As a result, capillary pressure curves cannot be directly obtained from this method [1].

MICP allows access to very small pores, but it does not allow for further use of the sample, and the fluid used may not be representative of the reservoir conditions [9]. It only provides information about the pore throats structure which is indirectly related to the resistivity index (RI)[15].

As another alternative, centrifuge provides a faster method of establishing saturation [9,10]. On the other hand, it is also limited in its ability to achieve true equilibrium conditions, particularly when applied to low-permeability samples and heterogeneous water saturation distributions resulting from the non-uniform distribution of capillary forces along the sample length [16]. Similarly to MICP, capillary pressure data is obtained by this method, rather than RI directly [17].

DRP, PNM, ANNs, and FT have developed various indirect methods for generating capillary pressure data [5,10–13,18–21], however, each approach has its own challenges and limitations.

* Corresponding author: Meysam.nourani@stratumreservoir.com

Among the challenges faced by DRP are data acquisition limitations, high computational demands, model simplifications, wettability representations, upscaling requirements, validation issues, and heterogeneity complexities [22–25].

Despite its significant potential, PNM is hindered by inaccuracies in pore network construction, difficulties in representing multiphase flow complexity, scaling issues and uncertainties in parameterization [26].

Although ANNs have potential for estimating capillary pressure curves, they experience several challenges, including a lack of physical constraints, the need for large, high-quality datasets, model complexity, difficulties with generalization, and high computational costs [5,26,27].

The use of FT for characterizing porous media and predicting capillary pressure is limited by difficulties in defining fractal dimensions, inherent model constraints, challenges in integrating wettability and fluid properties, high computational demands, complexities in upscaling and validation, and application-specific restrictions. [5,28,29]

Some of the alternatives mentioned earlier, such as MT, MICP, and centrifuge, are direct methods for measuring capillary pressure. However, as discussed, these methods face constraints in capturing true equilibrium and replicating reservoir conditions. Even though significant progress has been made in developing alternatives to PcRI measurement, the porous plate method remains the most effective method for determining capillary pressure and resistivity simultaneously. It is possible to retain the advantages of direct PcRI measurement while at the same time addressing its primary limitation, namely its significant time-consuming nature, by developing an alternative approach.

It was attempted to model the equilibrium process to accelerate the collection of porous-plate capillary pressure by not waiting for capillary equilibrium at each pressure step [1,30,31], which led to the invention of Short-Wait Porous Plate (SWPP) method [1]. This method is an advanced technique for simultaneously measuring capillary pressure and resistivity index. In contrast to the traditional equilibrium method, the SWPP eliminates the need for full saturation stabilization at every pressure step, which significantly reduces experimental time while maintaining accuracy. The SWPP method provides dynamic saturation and resistivity data by monitoring changes in resistivity during desaturation and predicting equilibrium saturations by using an exponential decay model. This approach is particularly effective in primary drainage scenarios, where piston-like fluid displacement ensures global water connectivity, minimizing errors caused by fluid trapping. The method has shown strong agreement with traditional equilibrium measurements and provides an approximate three-fold time saving over traditional equilibrium measurements, making it a valuable tool for the efficient characterization of reservoirs [1].

Despite its notable success, SWPP is subject to various constraints and difficulties that need to be thoroughly addressed for effective implementation. There is uncertainty regarding whether this method is applicable to other fluid and rock types, as most studies validating this method focus on oil/water systems and carbonate rocks. Additionally, the method does not specify the amount of data required for reliability, instead suggesting that the next step be increased only when the curve bends before proceeding.

Development of the models

Predicting equilibrium time and modelling the dynamic behaviour of resistivity and water production during PcRI tests is critical to optimize experimental workflows and ensuring high-quality data. This study utilizes a large dataset to evaluate a predictive approach for equilibrium time and transient resistivity behaviour in PcRI tests. By systematically analysing experimental PcRI data, this methodology enables accurate predictions of equilibrium time and dynamic system behaviour, improving the interpretation of PcRI test results. The findings demonstrate how predictive modelling can enhance laboratory workflows by reducing the duration of PcRI experiments while maintaining data quality. These results represent a significant step toward improving the efficiency and reliability of PcRI testing for broader applications in reservoir characterization. Within the framework of Archie's rock behaviour and its associated boundary conditions [32], we have developed analytical models to predict true resistivity and water production. These physics-based models are derived using analogies to electrical circuit behaviour, following a similar conceptual approach to those used for modelling the effect of clay on formation resistivity factor [33], as outlined below:

$$R_t = a_1 e^{-b_1 t} + c_1 \quad (1)$$

$$V_s = a_2 e^{-b_2 t} + c_2 \quad (2)$$

Although independently developed, the final expressions have an exponential decay form that is visually similar to those reported by Dernaika et al. [1]. The variables t, R_t and V_s are the time measurement, true resistivity of the sample and the amount of water produced, respectively. The constants a_1, a_2, b_1, b_2, c_1 and c_2 are all determined by fitting the model to the data using nonlinear least squares techniques.

Results and Discussion

At each capillary pressure step, true resistivity models are assumed to be independent of other capillary pressure steps. In this case, when transitioning to the next capillary pressure step, it is necessary to reset the true resistivity by setting the first registered resistivity to zero, which will serve as the base for that step. To calculate subsequent resistivity values, this base value must be subtracted from them. For the first example, Figure 1 shows a well-fitted resistivity model for the reset of true resistivity measured over 494 days at 275 mbar with an R^2 of 0.998. The equilibrium time for the model fitted to the true resistivity

data is 368 days. At the equilibrium time the true resistivity is 87.92 Ωm.

For the model to be effective, data on resistivity and the volume of fluids produced over time must be available. To verify the validity of the used models, macro programs were developed, and large data sets were fitted with the models. It was first examined how using different fluid systems such as crude oil/water, lab oil/water, and gas/water could affect the model's accuracy to predict true resistivity transients. Figures 2–4 present model validation results for different fluid pairs: crude oil/water (Example 2), lab oil/water (Example 3), and gas/water (Example 4). Each figure illustrates the correlation between predicted true resistivity and measured data for the respective system. Based on the cross plots in Figures 2-4, the model has been able to predict the true resistivity values for all three fluid systems with a good degree of accuracy. Based on the average relative error, the model demonstrates the highest accuracy for the gas/water system, with an average relative error of 5.6%, followed by the crude oil/water system (5.9%) and the laboratory oil/water system (8.5%).

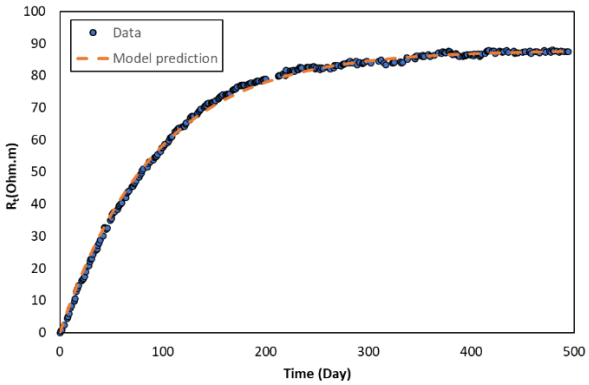

Fig. 1. Example 1, model fitting for true resistivity measurements over 494 days at 275 mbar, with an R^2 of 0.998. The dashed line indicates the model prediction.

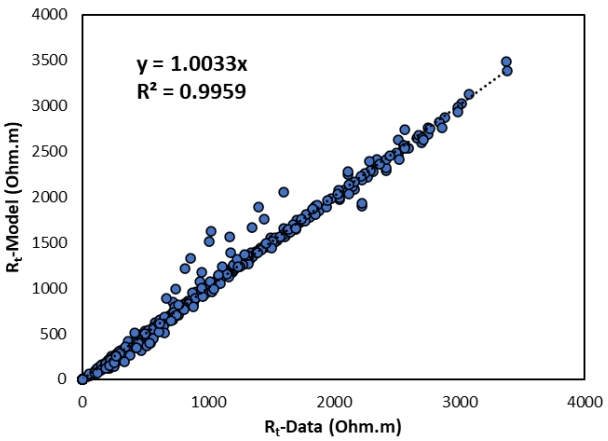

Fig. 2. Example 2, a comparison of the true resistivity calculated by the R_t model with the R_t data measured using the crude oil/water system was performed on plug samples containing 450 data points.

The second approach to validate the true resistivity model was to apply it to sandstone and carbonate samples and investigate their effects on the accuracy of the model in predicting true resistivity transients. For sandstone and carbonate samples, Figures 5 and 6 illustrate the correlation between true resistivity predictions and laboratory measured data. As shown in 5 and 6, the model accurately predicts the true resistivity values for both rock systems. However, the model provided slightly better predictions for the sandstone samples, with an average relative error of 5%, compared to 6% for the carbonate samples.

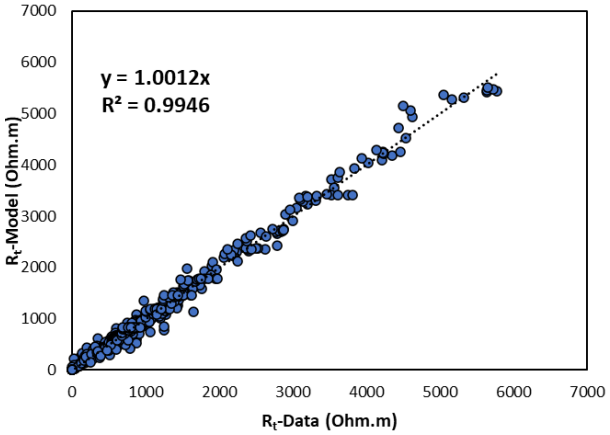

Fig. 3. Example 3, a comparison of the true resistivity calculated by the R_t model with the R_t data measured using the lab oil/water system was performed on plug samples containing 765 data points.

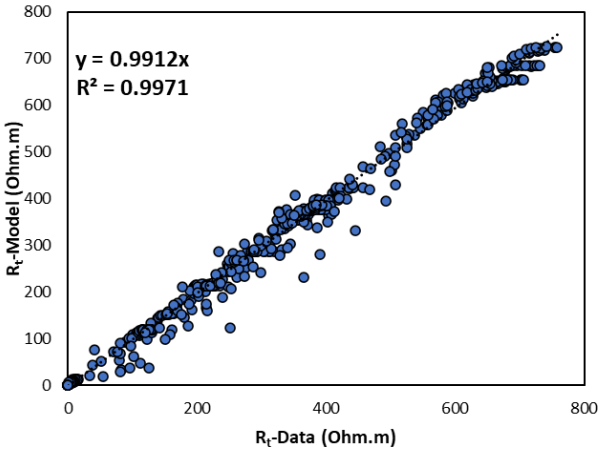

Fig. 4. Example 4, a comparison of the true resistivity calculated by the R_t model with the R_t data measured using the gas/water system was performed on plug samples containing 564 data points.

While fitting the developed models to this large dataset, it was observed that the R-squared value for the first pressure step consistently remained below 0.999, indicating lower prediction accuracy at this step. Figure 7 provides an example of this observation where water production and resistivity index (RI) data at the first pressure step are plotted along with their model predictions. This figure shows that the models were not able to predict well and deviated from the final values at day 60. This deviation in predicting true resistivity and water production at the first pressure step is likely due to the fact that, when oil flooding began, the oil had not yet reached the porous plate at the sample's outlet.

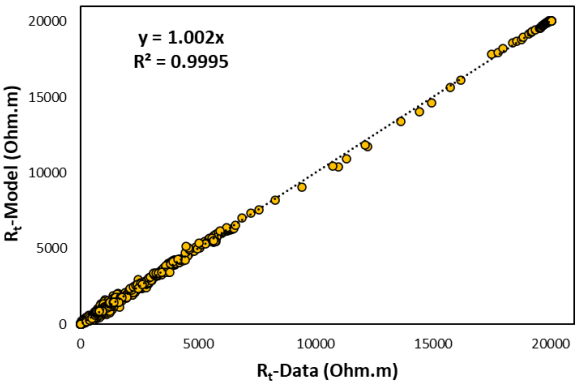

Fig. 5. Example 5, a comparison of the true resistivity calculated by the R_t model with the R_t data measured was performed on sandstone samples containing 9769 data points.

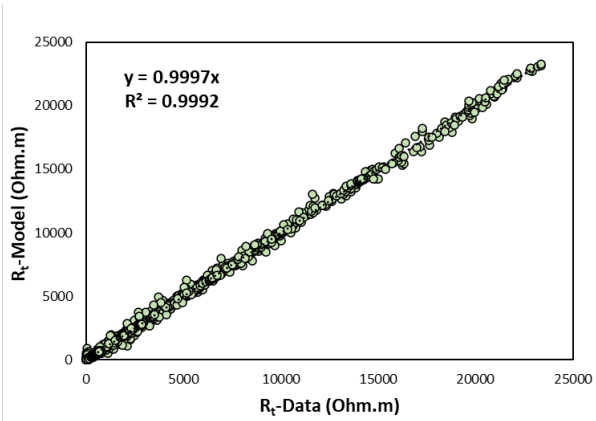

Fig. 6. Example 6, a comparison of the true resistivity calculated by the R_t model with the R_t data measured was performed on carbonate samples containing 2731 data points.

The R-squared is improved by removing some of the initial data and refitting the models. Removing more initial data points and refitting the models should be repeated until the highest R-squared has been achieved, indicating that the flooded oil has reached the end of the sample. An application of the developed models is to monitor the oil capillary dominated displacing mechanism and to identify when the oil reaches water-wet porous plate. Figure 8 illustrates that by removing the initial data in Figure 7 up to day 14, a much better model fit was achieved in predicting the final values.

Among the applications of the developed models, Figure 9 illustrates how the true resistivity model can be applied to correct anomalies in experimental data caused by equipment-related artifacts, rather than serving as a conventional model validation case. This example shows a PcRI measurement at 5,000 mbar capillary pressure, under net confining pressure (NCP), and at temperature. An unexpected equipment power failure on day 251 of the measurement resulted in the temperature dropping to an ambient level. When the technical issue was solved and the temperature was raised to reservoir conditions again, RI hysteresis effects were visible in the measured data, showing an increase of RI values after failure, and the trend of measurement changed as shown in Figure 9.

By feeding the true resistivity model with data collected before the failure, the model was able to predict the equilibrium value accurately, aligning with the original RI trend of the experiment.

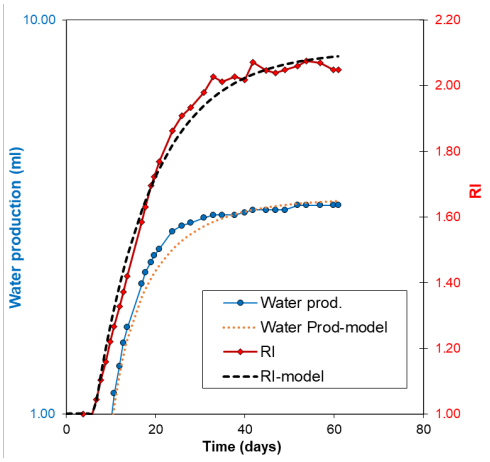

Fig. 7. Example 7, illustrating water production and RI data at the first pressure step alongside their model predictions, highlighting the models' less accurate performance and deviation from the final measured analytical values.

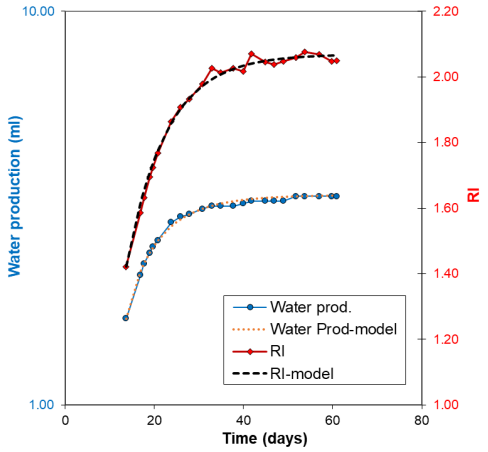

Fig. 8. Example 7, by excluding the initial data up to day 14 (same as in Figure 7), the model fitting significantly improved, resulting in better predictions of the final measured analytical values.

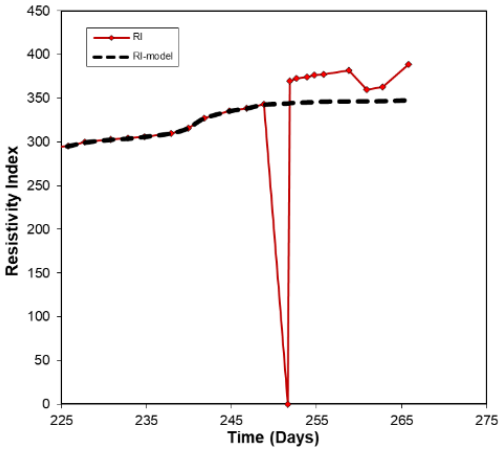

Fig. 9. Example 8, RI versus time for crude oil/water PcRI measurement at 5,000 mbar, NCP, and temperature. The true resistivity model (dashed line), based on pre-failure data, properly predicted the equilibrium value.

A significant detail to consider is that the equilibrium time for true resistivity and water production are different. Compared to true resistivity in PcRI measurements, water production reaches equilibrium faster since water flow is more directly responsive to pressure changes, whereas resistivity is affected by a slower process of water redistribution within the rock matrix, influenced by capillary pressure, fluid saturation distribution, wettability and rock properties.

Two different PcRI methods were conducted on a twin sample, A and B which are located only few centimeters apart. PcRI was conducted on sample A under NCP and temperature using an oil–water system with six capillary pressure steps of 50, 150, 500, 1,000, 2,500, and 5,000 mbar. The PcRI on sample B was conducted under the same NCP, temperature, and fluid conditions, but there were three pressure steps, 500, 2,500, and 5,000 mbar, where only equilibrium was achieved at the last pressure step, in contrast to sample A, which reached equilibrium at all pressure steps. As a result, the measurements on samples A and B are referred to as Multiple and Single, respectively. A time comparison reveals that sample A required 260 days for the Multiple measurement, whereas only 75 days were needed for the Single measurement. As presented in Table 1, the n-saturation exponent calculated from the Multiple experiment is 2.04, whereas it is 2.08 for the Single measurement.

The models were fitted to the transient water production and true resistivity data obtained from the Single measurement. Following the fitting, the experiment was extended to reach equilibrium time at 5,000 mbar, matching the duration of the Multiple measurement, as shown in Figures 10 and 11.

As shown in Figure 10, the multiple measurement was terminated prematurely at the final pressure step, before true resistivity had fully stabilized. However, as illustrated in Figure 11, water production had already reached sufficient stability. The RI at the final step was therefore predicted using the model, yielding a value of 1191, as reported in Table 1. As listed in Table 1, the final RI and irreducible water saturation (S_{wi}) achieved in the Multiple experiment were 1088 and 0.035 (frac), respectively. Based on the model's prediction for the Single method, the RI and water saturation were calculated as 1151 and 0.025 (frac), respectively. The final RI prediction using the Single method differed by 5% from the Multiple data and by 3% from the Multiple model.

Table 1. Final RI and S_{wi} values for the Multiple and Single methods, along with the model's predictions for the Single and Multiple method.

	B-Single (Data)	B-Single (Model)	A-Multiple (Data)	A-Multiple (Model)
Final RI	909	1151	1088	1191
S_{wi}	0.038	0.025	0.035	0.035
n	2.08	2.04	2.04	2.04

A comparison of MICP and PcRI data in low water saturation regions is presented in Figure 12. The model-derived estimate of final water saturation for the Single methodology closely matches the MICP data at 5,000 mbar.

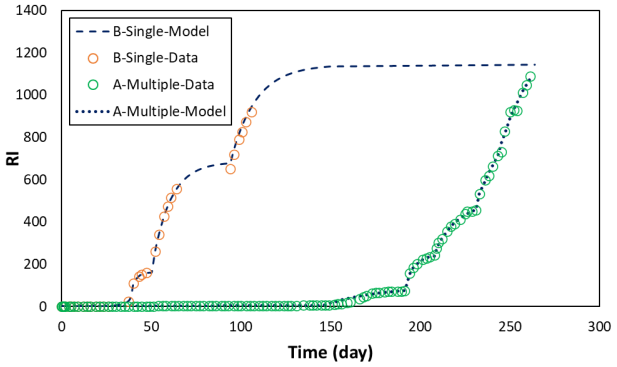

Fig. 10. Example 9, RI versus time for samples A and B at NCP and temperature. The model for true resistivity was fitted to the data, extending the experiment to estimate equilibrium for sample B (dashed line).

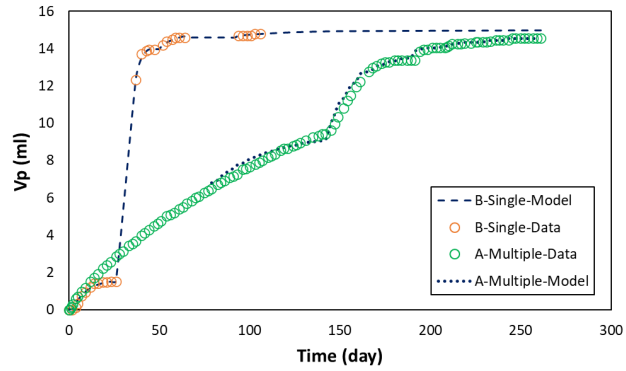

Fig. 11. Example 9, water production versus time for samples A and B at NCP and temperature. The model for water production was fitted to the data, extending the experiment to estimate equilibrium for sample B (dashed line).

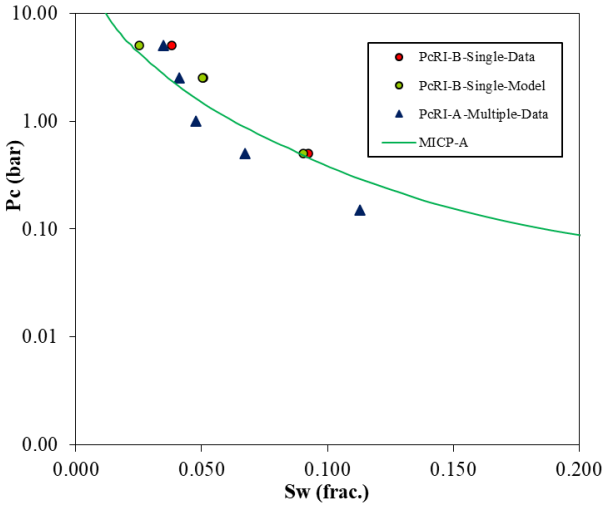

Fig. 12. Example 9, comparison of MICP and PcRI data in low water saturation regions for samples A and B.

The model output yielded a saturation exponent of 2.04, which matches the value obtained using the Multiple method, as illustrated in Figure 13. The availability of experimental data significantly influences model

accuracy, with greater data availability generally leading to improved estimations. However, reliable predictions require a minimum amount of data. By using statistical analysis, the models can predict equilibrium results with approximately 81% accuracy when data is collected for a period equal to 25% of the equilibrium period. Increasing the data collection period to 37% of equilibrium time improves the prediction accuracy to 99%. Thus, it is recommended that the PcRI time be at least 37% of equilibrium time to ensure a high degree of accuracy. This approach allows the models to accurately predict the equilibrium true resistivity and water production with sufficient transient production and resistivity data. Accordingly, if PcRI measurements are taken at a pressure step for 37% of equilibrium time, and the developed models are used to predict the results at equilibrium, up to 63% of the measurement time can be saved.

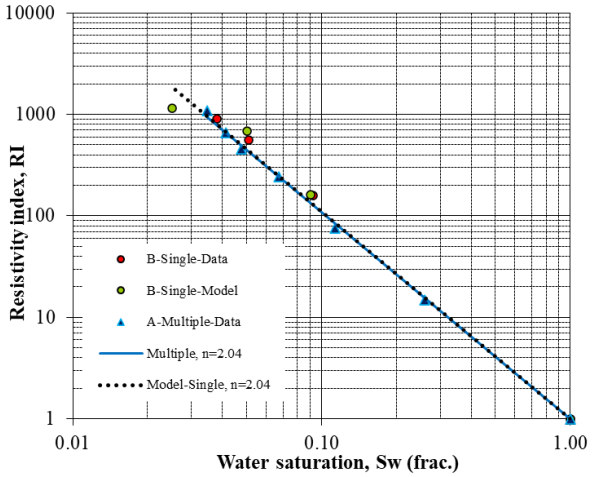

Fig. 13. Example 9, RI versus water saturation for samples A and B at NCP and temperature. Comparison of saturation exponents.

Conclusions

In conclusion, the developed exponential models demonstrate strong performance in predicting true resistivity and water production from PcRI measurements. Validation across a diverse range of sandstone and carbonate samples highlights their robustness, with slightly higher accuracy observed in sandstone formations.

Key advantages of these models include:

- Reliable data monitoring and quality control during PcRI measurements, ensuring consistency and integrity of results.
- Correction and adjustment capabilities for PcRI data in cases of equipment malfunction or data anomalies.
- High predictive accuracy, reducing measurement time by up to 63%, thereby enhancing laboratory efficiency and accelerating data delivery.
- Improved analysis and interpretation of PcRI results, facilitating more accurate reservoir characterization and efficient experimental data management.

Nomenclature

a_1	Fitting constant in Equation (1), Ωm
a_2	Fitting constant in Equation (2), ml
b_1	Fitting constant in Equation (1), day^{-1}
b_2	Fitting constant in Equation (2), day^{-1}
c_1	Fitting constant in Equation (1), Ωm
c_2	Fitting constant in Equation (2), ml
K	Permeability, mD
RI	Resistivity Index, dimensionless
R_t	Resistivity of rock partially saturated water, Ωm
t	Time, day
V_s	Volume of the water produced in the separator, ml

References

1. M. Dernaika, O.B. Wilson, S.M. Skjæveland, E. Ebeltoft, Petrophysics **57**, 369–376 (2016)
2. R.A. Adebayo, A. Isah, M. Mahmoud, D. Al-Shehri, Molecules **25**, 3385 (2020)
3. S. Pruno, H.E. Rodvelt, O. Skjæveland, E3S Web Conf. **89**, 02002 (2019)
4. N. Al-Bulushi, G. Kraishan, G. Hursan, Int. Pet. Technol. Conf. (IPTC), D021S045R004 (2019)
5. M. Saafan, T. Ganat, Fractals **29**, 2150149 (2021)
6. Q. Lin, B. Bijeljic, H. Rieke, M.J. Blunt, Water Resour. Res. **53**, 7457–7468 (2017)
7. D. Longeron, W.L. Hammervold, S.M. Skjaeveland, SPE Int. Oil Gas Conf. China, SPE-30006 (1995)
8. H.P.W. Zeelenberg, B.A. Schipper, Adv. Core Eval. II, 257 (1991)
9. I. Shikhov, C.H. Arns, SCA Symp., Napa Valley, USA, 16–19 (2013)
10. M. Al Hamad, D. Klemin, M.M. Shouxiang, W. Abdallah, SPE Middle East Oil Gas Show Conf., D011S121R005 (2023)
11. S. Bekri, C. Laroche, O. Vizika, SCA **35**, 2005 (2005)
12. H. Szűcs, B. Vehovszky, B. Sanders, Period. Polytech. Transp. Eng. **51**, 105–116 (2023)
13. M. Ba alawi, S. Gharbi, M. Mahmoud, Int. Pet. Technol. Conf. (IPTC), D031S075R002 (2020)
14. O.B. Wilson, S.M. Skjæveland, SCA Symp., Monterey, USA, SCA2002-016, 22–25 (2002)
15. Z. Tariq, M. Mahmoud, H. Al-Youssef, M.R. Khan, Pet. **6**, 35–42 (2020)
16. F. Pairoys, C. Caubit, M. Alexander, J. Ramos, E3S Web Conf. **366**, 1010 (2023)
17. I. Shikhov, C.H. Arns, Transp. Porous Media **107**, 623–640 (2015)

18. D. Bauer, S. Youssef, M. Han, S. Bekri, E. Rosenberg, M. Fleury et al., Phys. Rev. E **84**, 011133 (2011)
19. C. Chalbaud, M. Robin, J.M. Lombard, F. Martin, P. Egermann, H. Bertin, Adv. Water Resour. **32**, 98–109 (2009)
20. L. Algive, S. Békri, F.H. Nader, O. Lerat, O. Vizika, Oil Gas Sci. Technol. **67**, 147–160 (2012)
21. L. Jiao, J. Zhou, J. Cai, Capillarity **3**, 62–74 (2020)
22. H.P. Menke, Y. Gao, S. Linden, M.G. Andrew, Front. Water **4**, 935035 (2022)
23. A.B. Dixit, S.R. McDougall, K.S. Sorbie, J.S. Buckley, SPE Reserv. Eval. Eng. **2**, 25–36 (1999)
24. P.-R. Thomson, A. Aituar-Zhakupova, S. Hier-Majumder, Front. Earth Sci. (Lausanne) **6**, 58 (2018)
25. Q. Sheng, K. Thompson, Water Resour. Res. **49**, 5973–5988 (2013)
26. Q. Xiong, T.G. Baychev, A.P. Jivkov, J. Contam. Hydrol. **192**, 101–117 (2016)
27. A. Golparvar, Y. Zhou, K. Wu, J. Ma, Z. Yu, Adv. Geo-Energy Res. **2**, 418–440 (2018)
28. R.J. Cai, S.W. Tang, Z. He, Int. J. Eng. Sci. **123**, 143–157 (2018)
29. K. Li, J. Pet. Sci. Eng. **73**, 20–26 (2010)
30. J. Shafer, P. Lasswell, SPWLA Annu. Logging Symp., SPWLA-2007 (2007)
31. R. Lenormand, P. Delaplace, P. Schmitz, J. Pet. Sci. Eng. **19**, 93–102 (1998)
32. G.E. Archie, Trans. AIME **146**, 54–62 (1942)
33. M.H. Waxman, L.J.M. Smits, Soc. Pet. Eng. J. **8**, 107–122 (1968)